Clim Dyn (2018) 50:339–348
DOI 10.1007/s00382-017-3611-3

Seasonal prediction and predictability of Eurasian spring snow water equivalent in NCEP Climate Forecast System version 2 reforecasts

Qiong He[1,2] · Zhiyan Zuo[2,4] · Renhe Zhang[2,3] · Ruonan Zhang[2]

Received: 1 September 2016 / Accepted: 28 February 2017 / Published online: 29 June 2017

Abstract The spring snow water equivalent (SWE) over Eurasia plays an important role in East Asian and Indian monsoon rainfall. This study evaluates the seasonal prediction capability of NCEP Climate Forecast System version 2 (CFSv2) retrospective forecasts (1983–2010) for the Eurasian spring SWE. The results demonstrate that CFSv2 is able to represent the climatological distribution of the observed Eurasian spring SWE with a lead time of 1–3 months, with the maximum SWE occurring over western Siberia and Northeastern Europe. For a longer lead time, the SWE is exaggerated in CFSv2 because the start of snow ablation in CFSv2 lags behind that of the observation, and the simulated snowmelt rate is less than that in the observation. Generally, CFSv2 can simulate the interannual variations of the Eurasian spring SWE 1–5 months ahead of time but with an exaggerated magnitude. Additionally, the downtrend in CFSv2 is also overestimated. Because the initial conditions (ICs) are related to the corresponding simulation results significantly, the robust interannual variability and the downtrend in the ICs are most likely the causes for these biases. Moreover, CFSv2 exhibits a high potential predictability for the Eurasian spring SWE, especially the spring SWE over Siberia, with a lead time of 1–5 months. For forecasts with lead times longer than 5 months, the model predictability gradually decreases mainly due to the rapid decrease in the model signal.

Keywords CFSv2 · Eurasian spring SWE · Prediction · Predictability

1 Introduction

Snow cover is important for modulation of climatic variability and change (Namias 1985; Ellis and Leathers 1998). The presence of snow cover can affect the surface energy balance because of snow's high albedo and low conductivity. Furthermore, it can influence near-surface thermal characteristics and general atmospheric circulation (Robinson and Kukla 1984; Cohen 1994; Gong et al. 2004). Saito and Cohen (2003) proposed that snow cover contributes to the leading boreal winter mode of the atmosphere. Moreover, snow cover can affect the water balance during hydrologic processes, thereby influencing human activities (Yasunari et al. 2007). Many statistical analyses and numerical experiments have been used to identify the relationship between the Eurasian snow cover extent/depth and the rainfall of the Indian summer and East Asian monsoons (Yang and Xu 1994; Vernekar et al. 1995; Douville and Royer 1996; Sankar-Rao et al. 1996; Ferranti and Molteni 1999; Liu and Michio 2002; Singh and Oh 2005; Dash et al. 2006; Barnett et al. 2010). Wu and Kirtman (2007) found that excessive snow cover in western Siberia in spring is accompanied by above-normal spring rainfall in Southern China. The snow water equivalent (SWE) appropriately represents the global snow mass based on the effect of melting water on

✉ Zhiyan Zuo
zyzuo@camscma.cn

1 Earth System Modeling Center and Climate Dynamics Research Center, Nanjing University of Information Science & Technology, Nanjing, China

2 Skate Key Laboratory of Severe Weather, Chinese Academy of Meteorological Sciences, No 46 Zhongguancun South Street, Beijing 100081, China

3 Institute of Atmospheric Sciences, Fudan University, Shanghai, China

4 Collaborative Innovation Center on Forecast and Evaluation of Meteorological Disasters, Nanjing University of Information Science & Technology, Nanjing, China

the global climate (Souma and Wang 2010). Some studies have identified the impact of SWE, especially the SWE over Eurasia, on the Asian summer monsoon and precipitation (Dong and Valdes 2006; Wu et al. 2009; Chen et al. 2013; Xu and Wu 2012; Zuo et al. 2011). Zhang et al. (2008, 2013), Zuo et al. (2012) and Zuo and Zhang (2012) reported that the springtime SWE over Eurasia has a major impact on the spring and summer rainfall in China.

The NCEP Climate Forecast System version 2 (CFSv2) has been used for coupled ocean-atmosphere forecasts since 2011. This model is an upgraded version of CFSv1 that includes improvements to the model parameterization, initialization system, and resolution (Saha et al. 2014). Many studies have focused on prediction of MJO, sea ice extent, soil moisture, precipitation and 2-meter temperature using this system (Wang et al. 2012, 2013; Mo et al. 2012; Kim et al. 2012; Zuo et al. 2013, 2014). Apart from the study of He et al. (2016) which evaluated the prediction skill of Eurasian snow cover fraction using CFSv2 reforecasts, few studies have addressed the prediction capability of CFSv2 for snow properties, particularly the Eurasian SWE. Considering the great significance of the Eurasian spring SWE for the seasonal prediction of the Asian summer monsoon rainfall, we focus on the prediction skill of the Eurasian spring SWE using CFSv2 in terms of climatology, interannual variations, and potential predictability. The evaluation may be useful for the community to further upgrade the system and improve the simulation ability for snow variables. This paper is organized as follows: Sect. 2 briefly describes CFSv2 SWE reforecasts, the verification dataset, and the methods. Section 3 compares the Eurasian spring SWE climatology of CFSv2 with observations. Section 4 evaluates the prediction capability for interannual variations. Section 5 focuses on the potential predictability of the Eurasian spring SWE. A summary is provided in Sect. 6.

2 Data and methods

The present study is based on NCEP Climate Forecast System version 2 (CFSv2) reforecasts. This model is an improved version of CFSv1 and consists of the NCEP Global Forecast System (GFS) and the Modular Ocean Model version 4 (MOM4) coupled with a two-layer sea ice model and the Noah land surface model (Ek et al. 2003). It provides reforecasts for evaluation and calibration of model products. CFSv2 produces 9 month reforecasts initiated every 5 days with 00, 06, 12, and 18 Z cycles for the period 1982–2010. We focus on the Eurasian spring (March–May) SWE from CFSv2 reforecasts from 1983 to 2010. The assessment is based on the ensemble consisting of 16 members of each month for lead times of 1–9 months (LM0–8). For spring—the target predicted season (March–May)—0 month lead, the initial conditions of 10, 15, 20 and 25 February are for March, 12, 17, 22, 27 March are for April and 11, 16, 21, 26 April are for May. The initial conditions (ICs) of CFSv2 retrospective forecasts are from the NCEP Climate Forecast System Reanalysis (CFSR) (Saha et al. 2010, 2014). The snow liquid equivalent depth in the CFSR is updated using analysis data from the (i) Air Force Weather Agency's SNODEP model (Kopp and Kiess 1996) which uses in situ observations, an SSM/I-based detection algorithm and its own climatology and (ii) from the NESDIS IMS (Helfrich et al. 2007), which is a manually generated snow cover analysis produced once per day. IMS snow data were available at 23 km resolution staring in 1997 and at 4 km resolution staring in 2004 (Saha et al. 2010), which determined whether there was snow or not where there was disagreement with the SNODEP analyses.

The European Space Agency Data User Element GlobSnow-2 project is a direct continuation for the GlobSnow-1 project which aims at creating long-term records of snow cover information at the global scale intended for climate research purposes. The project is being coordinated by the Finnish Meteorological Institute (http://www.globsnow.info/index.php?page=Home). The GlobSnow-2 (hereafter GlobSnow) monthly SWE product is adopted as verification dataset that combines satellite-based passive microwave measurements with ground-based weather station data in the data assimilation system. It was derived from a newly developed assimilation approach that exhibited benefits compared with the typical stand-alone satellite passive microwave algorithm (Takala et al. 2011). There are evident that the assimilation approach improved the SWE estimation accuracy in about 60% of the investigated cases across Eurasia compared with the interpolation of weather station snow depth values only (Pulliainen 2006). Additionally, due to the uneven distribution and discontinuity in situ snow data, the long-term records of snow dataset with hemisphere scale, i.e. GlobSnow, is a prior option for climate research and model evaluation. It should also be noted that the GlobSnow SWE product is limited between the latitudes of 35°N and 85°N and mountainous regions in the GlobSnow products were masked out due to the poor algorithm performance in orographically complex regions (Takala et al. 2011). Moreover, the monthly satellite-derived SWE dataset provided by the National Snow and Ice Data Center (NCIDC) is also discussed in the analysis (Armstrong et al. 2005).

The statistical methods used in the analysis include the temporal correlation coefficient (TCC), pattern correlation coefficient (PCC), root-mean-square error (RMSE), and linear trend. Additionally, the present study is generally based on the ensemble mean prediction

averaged over 16 individual members. The signal-to-noise ratio (SNR) is defined as the relative magnitude of the variance of the ensemble mean to the variance of the departure of each member from the ensemble mean, which is used to investigate the potential predictability of CFSv2 (Peng et al. 2011).

3 Comparison of spring SWE climatology

First, we evaluate the capability of CFSv2 to forecast the climatological Eurasian spring SWE. Figure 1 shows the spatial pattern of the Eurasian spring SWE climatology from 1983 to 2010 in CFSv2 reforecasts for LM0–8 and the GlobSnow verification. The SWE is mainly concentrated over northern Eurasia, as demonstrated by a notably large center over western Siberia with the maximum SWE exceeding 180 mm and a second large center (maximum

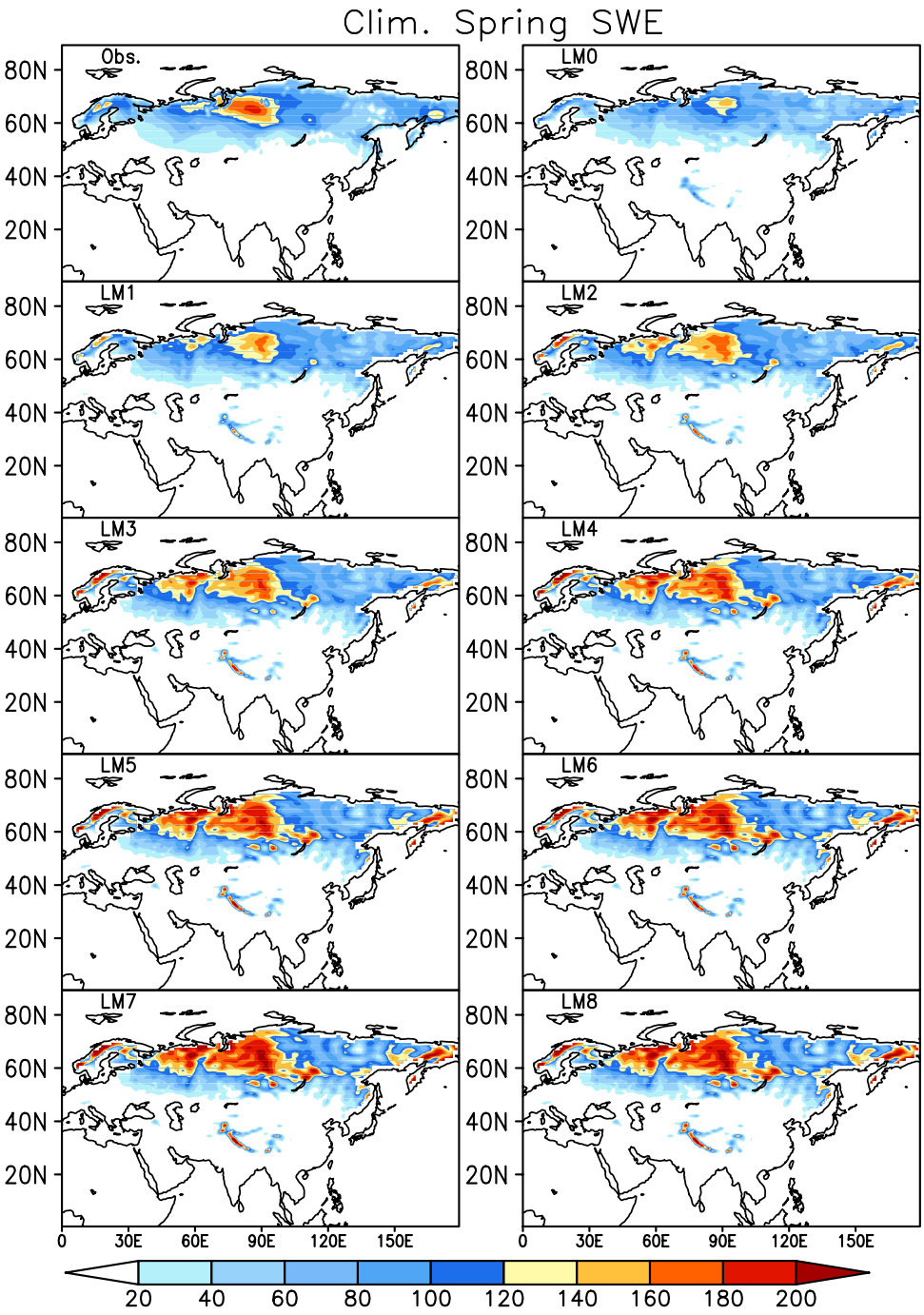

Fig. 1 Climatology of Eurasian spring SWE from GlobSnow and CFSv2 for LM0–8. The unit is mm

larger than 120 mm) over northeastern Europe. Generally, CFSv2 simulates a spatial distribution similar to that of the observed climatological Eurasian spring SWE. For example, CFSv2 for LM0–2 correctly captures the observed spatial distribution and the maximum of the SWE over western Siberia and northeastern Europe with a small bias. As the lead time increases, the forecasted SWE gradually increases, particularly over the two maximum centers. However, it reproduces the observed spatial pattern well. We calculate the PCCs for 0°–180°E, 40°–80°N of the climatology from the observation and CFSv2 for LM0–8. The PCCs are 0.90, 0.90, 0.89, 0.87, 0.85, 0.84, 0.84, 0.84, and 0.84 for LM0–8, respectively, confirming the strong simulation capability of CFSv2 for the climatological Eurasian spring SWE. Noticeably, the PCC gradually decreases for longer lead times, indicating relatively larger pattern bias for longer lead times. This is consistent with the results shown in Fig. 1, in which CFSv2 for LM0–2 exhibits an amplitude most similar to the observed Eurasian spring SWE climatology and the forecasted SWE increases with increasing forecast lead time, especially over the maximum center.

Figure 2a quantitatively describes the averaged climatological spring SWE over Eurasia (0°–180°E, 40°–80°N) from CFSv2 for LM0–8 (color bars) and the observation (black bar). CFSv2 reforecasts simulate the mean Eurasian spring SWE more accurately for LM0–2 and gradually overestimate it for longer lead times. Specifically, the observed mean spring SWE over Eurasia is approximately 49.5 mm, and CFSv2 for LM0–2 has only a −4.2 to 10.2 mm bias. Note that the underestimated SWE in the CFSv2 for LM0 is probably caused by the negative bias of the CFSR compared with the GlobSnow (seen in Fig. 3) since the model has only integrated for 1 month and the effect of initial condition is dominant. As the lead time increases, the bias also increases, exhibiting 16.5–28.5 mm larger values than the observation for LM3–8. The analysis of the model simulation for the mean Eurasian spring 2-meter temperature shows that CFSv2 produces more and more lower-than-observed surface temperatures (results not shown) when the lead time increases. Previous studies have demonstrated that the spring snow cover retreat may lead to a positive feedback on the surface temperature and that the spring snowmelt depends on temperature (Groisman et al. 1994; Namias 1985). The underestimation of the spring 2-meter temperature may explain the generally excessive SWE of the model. However, the overestimation of the SWE may be the cause of the lower-than-observed 2-meter temperature in CFSv2. Furthermore, the treatment of the snowpack in the snow-related physics of the Noah LSM affects the surface skin temperature and in turn depends on the surface temperature (Ek et al. 2003). Thus, it is necessary to further improve the parameterization of the snow-related physics in the Noah LSM.

To specifically examine the model simulation for the SWE change in each month during springtime, we further calculate the SWE change in March, April, and May relative to the previous month in the observation (Fig. 2b, leftmost black bar) and CFSv2 for LM0–8 (Fig. 2b, colored

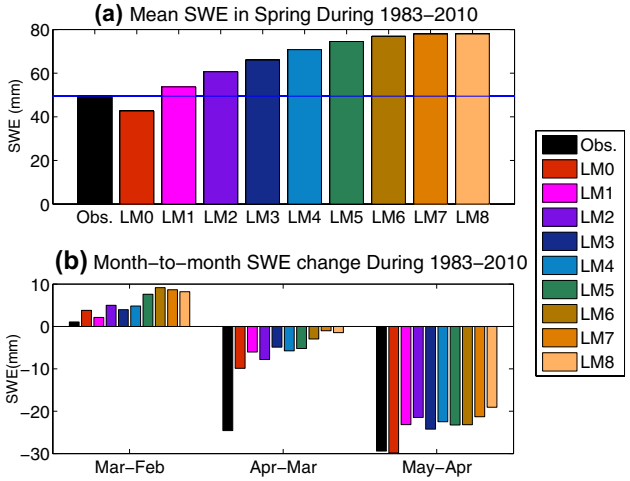

Fig. 2 Eurasian SWE (averaged over 0°E–180°E, 40°N–80°N) (**a**) in spring and month-to-month SWE changes (**b**) in March (March−February), April (April−March) and May (May−April) from GlobSnow and CFSv2. The unit is mm

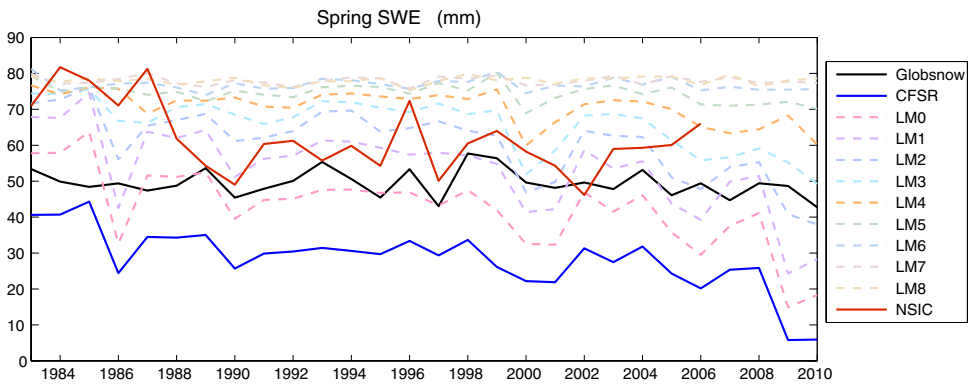

Fig. 3 Time series of spring SWE averaged over Eurasia (0°–180°E, 40°–80°N) from GlobSnow (*black solid line*), CFSR (*blue solid line*), CFSv2 for LM0–8 (*colored dashed lines*) for 1983–2010 and NSIDC (*red solid line*) for 1983–2006. The unit is mm

bars). The positive values reflect the climatological SWE increase, whereas the negative values refer to the climatological SWE decrease. The SWE increases in March and decreases in April and May both in the observation and CFSv2. However, the observed SWE increase in March is quite small (1.06 mm), whereas CFSv2 predicts a higher SWE increase (2.12–9.16 mm) for all lead times. The observed SWE decrease during April is quite extensive (24.60 mm), but CFSv2 predicts only less than half the observational SWE decrease (1.02–9.87 mm). The forecasted excessive snow accumulation in March and smaller snow ablation in April suggest that CFSv2 predicts a later start of snowmelt and a smaller snowmelt rate than the observation. This is most likely the reason for the forecasted excessive spring SWE in the model, which is consistent with the results from Zuo et al. (2014). On the other hand, the later start of snowmelt in CFSv2 is probably due to the choice of GlobSnow as verification dataset, for Mudryk et al. (2015) found that GlobSnow, with maximum SWE during late February to early March, peaks earlier than other four reanalysis datasets. Thus, the smaller snowmelt rate in the CFSv2 is probably the prominent cause for the overestimated spring SWE.

4 Prediction of the interannual variability

A critical issue in assessing CFSv2 reforecasts is the choice of verification data. In addition to the GlobSnow SWE verification, we also investigate different SWE data from the CFSR and NSIDC. Figure 3 shows the time series of spring SWE averaged over Eurasia (0°–180°E, 40°–80°N) from CFSv2, GlobSnow, CFSR for 1983–2010 and NSIDC for 1983–2006. The black, red, and blue solid lines represent the SWE from GlobSnow, NSIDC, and CFSR, respectively; the dotted lines are CFSv2 reforecasts for LM0–8. All of these SWE series exhibit notable interannual variations except CFSv2 for LM5–8. Noticeably, the SWE series from CFSv2 and CFSR exhibit almost the same variation. The correlation coefficients of CFSv2 for LM0–2 and CFSR are 0.98, 0.97, and 0.93, indicating a close relationship between the model results and the CFSR. This manifests in the successful forecasts of CFSv2 but also demonstrates the model dependence on the ICs significantly. Considering the possible link between the CFSR and CFSv2 products, we did not use the CFSR as verification dataset. Furthermore, a correlation analysis indicates that the disagreement between GlobSnow and NSIDC SWE is quite large, with the correlation coefficient between them equal to 0.16. There is evidence that the algorithm that the GlobSnow SWE is based on is more accurate than the other currently available existing algorithms (Luojus and Pulliainen 2010). The GlobSnow dataset is currently the best global SWE product when comparing it with the NSIDC SWE, especially because the latter exhibits spurious features during snowmelt (Hancock et al. 2013). Thus, we do not use the NSIDC SWE as the verification dataset in this paper. In a short, we used the GlobSnow product as the verification dataset for objective and independent evaluation.

Figure 3 shows that as the lead time increases, the time series values of the Eurasian spring SWE in CFSv2 reforecasts also increase and are generally larger than the GlobSnow observation. The prediction capability is calculated as the TCC and RMSE compared with the GlobSnow SWE. Table 1 gives the TCC and normalized RMSE between the anomalies from CFSv2 for LM0–8 and the observations. Notably, the TCC for LM0–4 is significant (>90% confidence level) and gradually decreases with increasing lead time. The RMSE for LM0–4 is <1 and gradually increases to be >1 as the lead time becomes longer. The greater TCC and smaller RMSE indicate higher predictive skill, suggesting that CFSv2 has a high predictive capability for the Eurasian spring SWE, 1–5 months ahead, with a relatively higher correlation with the observation and a moderate model bias. When the lead time is longer than 5 months, CFSv2 gradually loses the prediction skill for the interannual variations, and the interannual biases between model and observation considerably increase.

CFSv2 seems to produce a more significant decreasing trend for LM0–4 than the observed SWE and exhibits notable interannual variations. As the forecast lead time increases, the SWE interannual variation amplitude in CFSv2 tends to damp and no longer exhibits a significant trend. To compare the forecasted and observed variability and linear trend quantitatively, Fig. 4 illustrates the standard deviation (Fig. 4a) and linear trend (Fig. 4b) of the Eurasian spring SWE from the observation (black bars) and CFSv2 for LM0–8 (blue bars). Noticeably, CFSv2 for LM0–4 exhibits a more significant decreasing trend of the Eurasian spring SWE compared with the GlobSnow

Table 1 Correlation coefficients of the Eurasian spring SWE between GlobSnow and CFSv2 for LM0–8 and the RMSE between them

	LM0	LM1	LM2	LM3	LM4	LM5	LM6	LM7	LM8
R	**0.36**	**0.33**	**0.38**	**0.38**	**0.4**	0.29	0.22	−0.1	−0.1
RMSE	0.92	0.93	0.91	0.92	0.99	1.47	2.19	3.5	3.53

Bold numbers represent >90% confidence levels (Student's T-test)

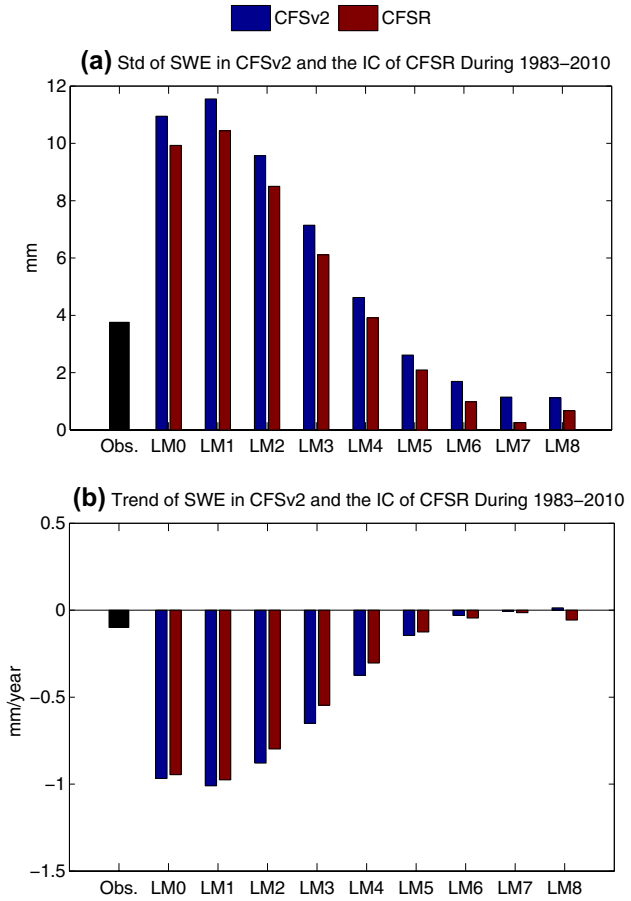

Fig. 4 Standard deviation (**a**, units: mm) and linear trend (**b**, units: mm/year) of Eurasian spring SWE in the observation (*black bars*), CFSv2 for LM0–8 (*blue bars*) and their initial conditions in CFSR (*red bars*) of the model

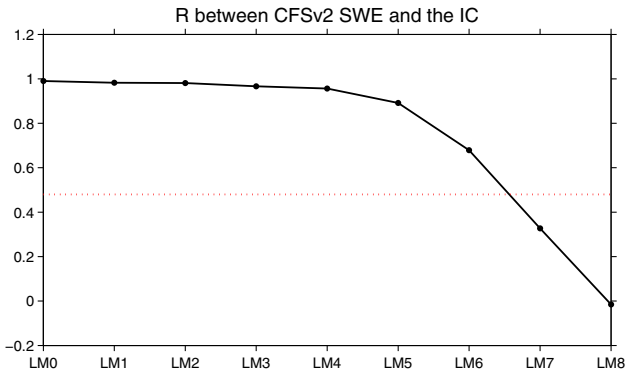

Fig. 5 Correlation coefficients of CFSv2 Eurasian spring SWE for LM0–8 and the respective initial conditions in CFSR. The *red short dashed line* is the threshold value of 99% confidence level

verification (Fig. 4b). And Affected by the simulated overestimated downtrend in the model, it also exhibits overlarge variability for LM0–4 (Fig. 4a). Specifically, the observed linear trend of the Eurasian spring SWE is −0.10 mm/year. However, CFSv2 for LM0–4 predicts a much more significant downtrend, with a trend value of −0.37 to −1.01 mm/year. The standard deviation of the observed Eurasian spring SWE is slightly less than 4 mm, whereas that of CFSv2 for LM0–4 ranges from 4.62 to 11.5 mm. The standard deviation of LM5–8 damps to smaller values than the observation (1.6–2.61 mm), with the linear trend becoming insignificant. Overall, the forecasted variability and trend value of the Eurasian spring SWE from CFSv2 for LM0–4 are significantly greater than those of the observation. As the lead time increases, both of them rapidly decrease and even approach zero for LM5–8. Some studies have found that the results tend to approximate the climatology when the models are integrated for a long period (e.g. Peng et al. 2011), which may partly explain the near-zero interannual magnitude of the Eurasian spring SWE for LM6–8 in CFSv2.

Previous studies found that snow initialization has a large impact on the model prediction skill (Wood and Lettenmaier 2008; Shongwe et al. 2007; Jeong et al. 2013; Orsolini et al. 2013). Does the Eurasian spring SWE variation in CFSv2 depend on the ICs? If so, to what extent does it depend on the ICs? To answer these questions, we report the Eurasian spring SWE standard deviation and linear trend in the corresponding ICs of the model (red bars in Fig. 4a, b). Specifically, the ICs of the spring (March–May) SWE in CFSv2 reforecasts for LM0, LM1, LM2, LM3, LM4, LM5, LM6, LM7, and LM8 are the SWE from CFSR during February–April, January–March, December–February, November–January, October–December, September–November, August–October, July–September, and June–August, respectively. A comparison of the blue and red bars in Fig. 4a, b reveals that the forecasted standard deviation and trend of the Eurasian spring SWE are almost equivalent to those of their respective ICs. Additionally, as the lead time changes, the standard deviation and trend surprisingly vary with the same change feature. Furthermore, we calculate the correlation coefficients of the spring SWE in CFSv2 for LM0–8 and their corresponding ICs to explore the probable linkage of the model forecasts and the ICs (Fig. 5). Figure 5 shows that CFSv2 for LM0–6 has a significantly strong correlation with the ICs (exceeding the 99% confidence level). In particular, for LM0–4, the TCCs are 0.99, 0.98, 0.98, 0.97, and 0.96, indicating a rather high dependence of the model results on their ICs 1–5 months ahead. When the lead time is longer than 7 months, the correlation gradually becomes insignificant. This suggests that the influence of the ICs becomes weaker after integrating long enough. Therefore, Eurasian spring SWE in CFSv2 for LM0–4 depends on the ICs significantly. We speculate that the overestimated interannual variability and the significant

negative trend in CFSv2 for LM0–4 are driven by the corresponding ICs. Nevertheless, since the CFSR SWE input data also include in-situ observed data and the standard deviation and trend of SWE from CFSR are much larger than those from GlobSnow, the overestimated interannual variability and negative trend may be caused by the different input datasets and assimilation algorithms between the two datasets.

5 Predictability of the spring SWE

As the lead time increases for the ensemble prediction starting from 16 slightly different SWE ICs, the discrepancies between the individual members of the ensemble become larger. In other words, the forecast spread would be small for a shorter lead time and become larger with increasing lead time. The relative magnitude of the ensemble mean variance (EMV) to the forecast spread is defined as the signal-to-noise ratio (SNR), which is used to analyze the potential model predictability. A greater SNR indicates a higher potential predictability, and a SNR of less than 1 reflects no predictability.

Figure 6 shows the spatial SNR of the Eurasian spring SWE in CFSv2 for LM0–7. For the shortest lead time of 1 month, the SNR of Eurasia is almost greater than 2, suggesting a high predictability after integrating for 1 month. In particular, the largest SNR is mainly located over

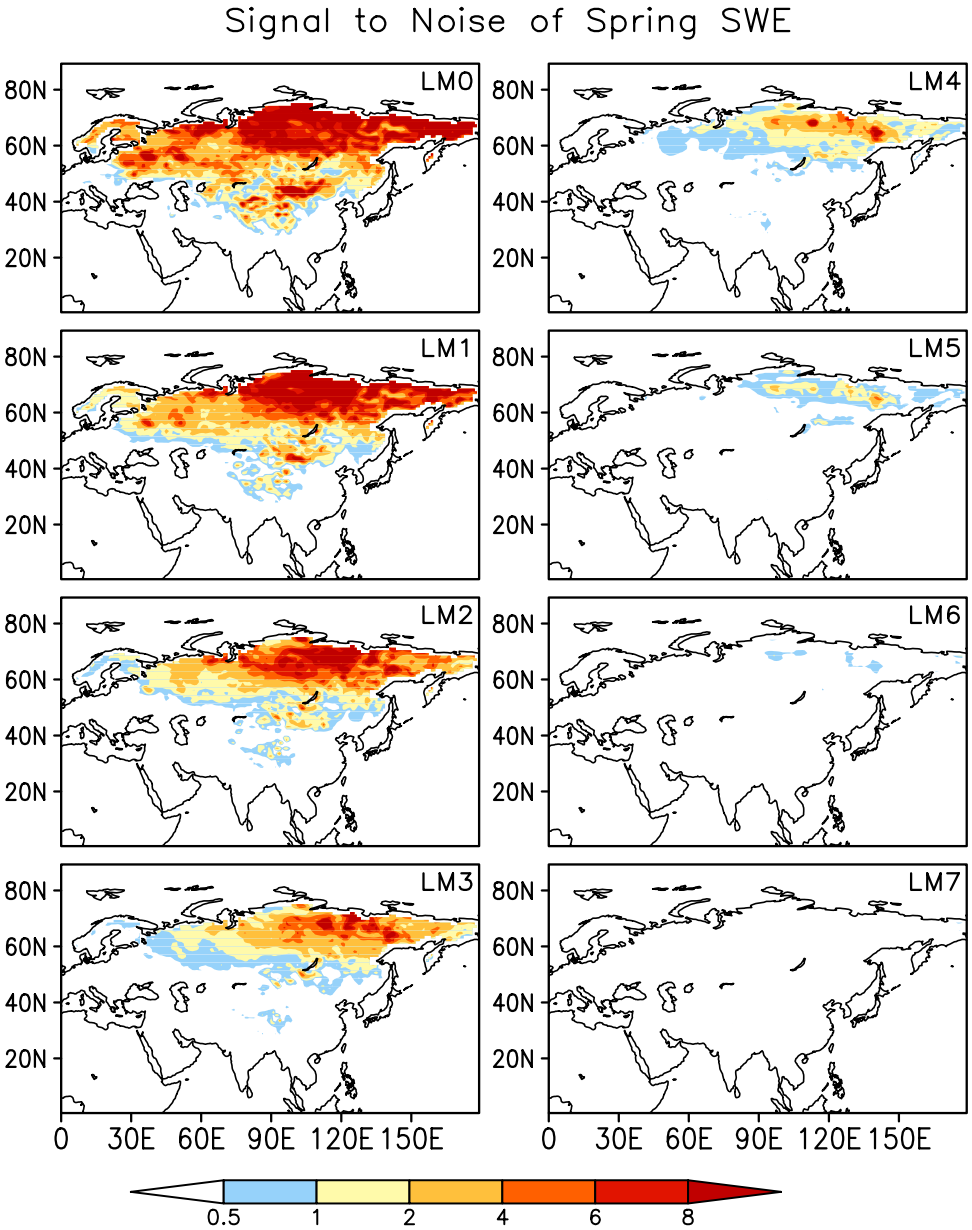

Fig. 6 SNR of Eurasian spring SWE in CFSv2 for LM0–7

Siberia, with a maximum greater than 8, suggesting that CFSv2 has the highest predictability for the spring SWE over Siberia compared with other areas of Eurasia. As the lead time increases, the area with SNR exceeding one gradually retreats northward, and the SNR becomes smaller. Up to a lead time of 5 months, CFSv2 exhibits predictability for most parts of Siberia. When the lead time is longer than 5 months, the SNR is less than one, indicating little predictability of the model for the Eurasian spring SWE. Overall, CFSv2 has potential predictability for the Eurasian spring SWE for a lead time of 1–5 months. When the lead time is longer than 5 months, it tends to lose predictive power for the spring SWE for whole Eurasia.

A summary of the lead time dependence of the model signal, noise, and SNR is shown in Fig. 7, in which the square root of the SWE EMV (signal), forecast spread (noise), and their ratio based on the average Eurasia spring SWE are illustrated. The SNR is greater than one for LM0–4 and becomes less than one for longer lead times, which is in good agreement with Fig. 6. Noticeably, the square root of EMV declines sharply with increasing lead time. For example, the square root of EMV of LM5–8 is almost only one-fourth of that of LM0. In contrast, the forecast spread stays almost constant, with the square root of the internal variance being approximately 3 mm, as the lead time increases. This result indicates that the forecast spread among the ensemble members grows quickly. The square root of forecast spread has increased to 3 mm, even when integrating only 1 month, and changes little with the increasing lead time. Therefore, we conclude that it is the rapid decrease of the EMV together with the constantly large forecast spread that causes the damping of the SNR of the Eurasian spring SWE in CFSv2 for the longer lead tim.

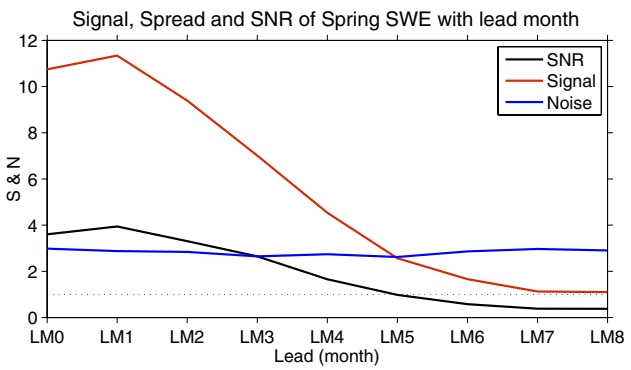

Fig. 7 Lead time dependence of the square root of the SWE EMV (*red curve*), forecast spread (*blue curve*) and the SNR (*black curve*) of Eurasian spring SWE (averaged over 40°–80°N, 0°–180°E). The LM of the forecast is indicated on the *x*-axis

6 Summary

The seasonal prediction capability and predictability for the Eurasian spring SWE and its evolvement with the lead time are evaluated using retrospective forecasts from NCEP CFSv2. The simulation ability of long-term climatology, interannual variation, and the predictability were assessed. Generally, CFSv2 reforecasts have predictive capability and predictability in the Eurasian spring SWE 1–5 months in advance.

CFSv2 realistically reproduces the observed climatological Eurasian spring SWE pattern, with two large centers located over Siberia and northeastern Europe. CFSv2 could correctly simulate the climatological Eurasian spring SWE for a lead time of 1–3 months, with a large pattern correlation coefficient and a small bias. As the lead time increases, the model gradually produces an excessive SWE compared with the observation. This is most likely because of the later snowmelt initiation and the smaller snowmelt rate in the model. Furthermore, because the surface temperature plays an important role in the snowmelt process, we also assessed the simulation capability of CFSv2 for the mean Eurasian spring 2-meter temperature. The results demonstrate that the model predicts a lower-than-observed 2-meter temperature during springtime. We can speculate that it is the underestimation of the 2-meter temperature in CFSv2 that hinders the snowmelt initiation and decreases the snowmelt rate, eventually leading to the excessive SWE in the model. The snowmelt process also affects the surface temperature. The interaction between the snow and surface temperature is quite complicated, and further studies are needed. Overall, it is crucial to understand the snow-temperature relationship and improve the snow-related parameterization in the Noah LSM.

CFSv2 reforecasts for LM0–4 could forecast the interannual variation of the Eurasian spring SWE significantly, with the correlation coefficients exceeding the 90% confidence level and RMSEs smaller than 1. However, there are still biases in the interannual variation compared with the observation. For example, the interannual variability and decrease trend of the Eurasian spring SWE in CFSv2 for LM0–4 are larger than the observed. Because the relationship between the Eurasian spring SWE from the model prediction and their corresponding ICs of CFSR are significant (exceeding the 99% confidence level for LM0–4), the standard deviation and linear trend of them are similar. In other words, the robust interannual variability and the downtrend in the ICs may be the causes for the overestimation of the interannual variability and decrease trend in the model. Thus, in addition to the snow-related parameterization, it is also necessary to further improve the initialization system of CFSv2 for better simulation. The results also demonstrate that CFSv2 has a high potential predictability

for the Eurasian spring SWE for a lead time of 1–5 months, with a SNR greater than one over most of Eurasia. CFSv2 has the highest potential predictability over Siberia. For predictions beyond 5 month, the SNR decreases below one, indicating no predictability for the Eurasian spring SWE.

Acknowledgements This study was jointly supported by the National Key Research and Development Program (Grant No. 2016YFA0601502), the National Natural Science Foundation of China (Grant Nos. 41205059, 41221064, 41375092) and the Basic Research Fund of the Chinese Academy of Meteorological Sciences (Grant No. 2015Z001).

References

Armstrong RL, Brodzik MJ, Knowles K, Savoie M (2005) Global monthly EASE-grid snow water equivalent climatology. National Snow and Ice Data Center, digital media, Boulder

Barnett TP, Dümenil L, Schlese U et al (2010) The effect of Eurasian snow cover on regional and global climate variations. J Atmos Sci 46(5):661–686

Chen H, Duo Q, Bei X (2013) Influence of snow melt anomaly over the mid–high latitudes of the Eurasian continent on summer low temperatures in northeastern China. Chin J Atmos Sci 37(6):1337–1347 (**Chinese**)

Cohen J (1994) Snow cover and climate. Weather 49(5):150–156

Dash SK, Sarthi PP, Panda SK (2006) A study on the effect of Eurasian snow on the summer monsoon circulation and rainfall using a spectral GCM. Int J Climatol 26(8):1017–1025

Dong B, Valdes PJ (2006) Modelling the Asian summer monsoon rainfall and Eurasian winter/spring snow mass. Q J R Meteorol Soc 124(124):2567–2596

Douville H, Royer JF (1996) Sensitivity of the Asian summer monsoon to an anomalous Eurasian snow cover within the Météo-France GCM. Clim Dyn 12(7):449–466

Ek MB, Mitchell KE, Lin Y, Rogers E, Grunmann P, Koren V, Gayno G, Tarpley JD (2003) Implementation of Noah land surface model advances in the national centers for environmental prediction operational mesoscale Eta model. J Geophys Res 108:8851. doi:10.1029/2002JD003296

Ellis AW, Leathers DJ (1998) The effects of a discontinuous snow cover on lower atmospheric temperature and energy flux patterns. Geophys Res Lett 25(12):2161–2164

Ferranti L, Molteni F (1999) Ensemble simulations of eurasian snow-depth anomalies and their influence on the summer Asian monsoon. Q J R Meteorol Soc 125(559):2597–2610

Gong G, Entekhabi D, Cohen J et al (2004) Sensitivity of atmospheric response to modeled snow anomaly characteristics. J Geophys Res 109(6):471–475

Groisman PY, Karl TR, Knight RW et al (1994) Changes of snow cover, temperature, and radiative heat balance over the northern hemisphere. J Clim 7(11):1633–1656

Hancock S, Baxter R, Evans J et al (2013) Evaluating global snow water equivalent products for testing land surface models. Remote Sens Environ 128(1):107–117

He Q, Zuo ZY, Zhang RH, Yang S, Wang WQ, Zhang RN, Riddle E (2016) Prediction skill and predictability of Eurasian snow cover fraction in the NCEP Climate Forecast System version 2 reforecasts. Int J Climatol 36:4071–4084. doi:10.1002/joc.4618

Helfrich SR, McNamara D, Ramsay BH, Baldwin T, Kasheta T (2007) Enhancements to, and forthcoming developments in the interactive multisensor snow and Ice Mapping System (IMS). Hydrol Processes 21:1576–1586. doi:10.1002/hyp.6720

Jeong JH, Linderholm HW, Woo SH et al (2013) Impacts of snow initialization on subseasonal forecasts of surface air temperature for the cold season. J Clim 26(51):1956–1972. doi:10.1175/JCLI-D-12-00159.1

Kim HM, Webster PJ, Curry JA (2012) Seasonal prediction skill of ECMWF system 4 and NCEP CFSv2 retrospective forecast for the northern hemisphere winter. Clim Dyn 39:2957–2973. doi:10.1007/s00382-012-1364-6

Kopp TJ, Kiess RB (1996) The Air Force Global Weather Central snow analysis model. In: Preprints, 15th conference on weather analysis and forecasting, Norfolk, VA, Amer Meteor Soc 220–222

Liu X, Michio Y (2002) Influence of Eurasian spring snow cover on Asian summer rainfall. Int J Climatol 22(9):1075–1089

Luojus K, Pulliainen J et al (2010) ESA DUE GlobSnow — global snow database for climate research. ESA Living Planet Symposium, June 28–July 2, Bergen Norway

Mo KC, Shukla S, Lettenmaier DP et al (2012) Do climate forecast system (CFSv2) forecasts improve seasonal soil moisture prediction? Geophys Res Lett 39:L23703. doi:10.1029/2012GL053598

Mudryk LR, Derksen C, Kushner PJ et al (2015) Characterization of northern hemisphere snow water equivalent datasets, 1981–2010. J Clim. doi:10.1175/JCLI-D-15-0229.1

Namias J (1985) Some empirical evidence for the influence of snow cover on temperature and precipitation. Mon Weather Rev 113 1542–1553

Orsolini YJ, Senan R, Balsamo G, et al (2013) Impact of snow initialization on sub-seasonal forecasts. Clim Dyn 41(7–8):1–14. doi:10.1007/s00382-013-1782-0

Peng P, Kumar A, Wang W (2011) An analysis of seasonal predictability in coupled model forecasts. Clim Dyn 36:637–648. doi:10.1007/s00382-009-0711-8

Pulliainen J (2006) Mapping of snow water equivalent and snow depth in boreal and sub-arctic zones by assimilating space-borne microwave radiometer data and ground-based observations. Remote Sens Environ 101:257–269

Robinson DA, Kukla G (1984) Albedo of a dissipating snow cover. J Clim Appl Meteorol 23(12):1626–1634

Saha S, Moorthi S, Pan H-L et al (2010) The NCEP climate forecast system reanalysis. Bull Am Meteorol Soc 91:1015–1057. doi:10.1175/2010Bams3001.1

Saha S et al (2014) The NCEP Climate Forecast System version 2. J Clim 27:2185–2208. doi:10.1175/JCLI-D-12-00823.1

Saito K, Cohen J (2003) The potential role of snow cover in forcing interannual variability of the major northern hemisphere mode. Geophys Res Lett 30(6):293–293

Sankar-Rao M, Lau KM, Yang S (1996) On the relationship between Eurasian snow cover and the Asian summer monsoon. Int J Climatol 16(6):605–616

Shongwe ME, Ferro CAT, Coelho CAS, et al (2007) Predictability of cold spring seasons in Europe. Mon Weather Rev 135(12):4185–4201. doi:10.1175/2007MWR2094.1

Singh GP, Oh JH (2005) Study on snow depth anomaly over Eurasia, Indian rainfall and circulations. J Meteorol Soc Jpn Ser ii 83(2):237–250

Souma K, Wang Y (2010) A comparison between the effects of snow albedo and infiltration of melting water of Eurasian snow on East Asian summer monsoon rainfall. J Geophys Res Atmos 115:D02115. doi:10.1029/2009JD012189

Takala M, Luojus K, Pulliainen J et al (2011) Estimating northern hemisphere snow water equivalent for climate research through assimilation of space-borne radiometer data and ground-based measurements. Remote Sens Environ 115(12):3517–3529

Vernekar AD, Zhou J, Shukla J (1995) The effect of Eurasian snow cover on the Indian monsoon. J Clim 8(2):248–266

Wang W, Huang MP, Weaver SJ, Kumar A, Fu XH (2012) MJO prediction in the NCEP Climate Forecast System version 2. Clim Dyn 42(9–10):2509–2520. doi:10.1007/s00382-013-1806-9

Wang W, Chen M, Kumar A (2013) Seasonal prediction of Arctic sea ice extent from a coupled dynamical forecast system. Mon Weather Rev 141:1375–1394

Wood AW, Lettenmaier DP (2008) An ensemble approach for attribution of hydrologic prediction uncertainty. Geophys Res Lett 35(14):159–169. doi:10.1029/2008GL034648

Wu R, Kirtman BP (2007) Observed relationship of spring and summer east Asian rainfall with winter and spring Eurasian snow. J Clim 20(7):1285–1304

Wu B, Yang K, Zhang R (2009) Eurasian snow cover variability and its association with summer rainfall in China. Adv Atmos Sci 26:31–44

Xu L, Wu B (2012) Linkage between spring Eurasian snowmelt and East Asian summer monsoon. Chin J Atmos Sci 36(6):1180–1190

Yang S, Xu L (1994) Linkage between Eurasian winter snow cover and regional Chinese summer rainfall. Int J Climatol 14(7):739–750

Yasunari T, Kitoh A, Tokioka T (2007) Local and remote responses to excessive snow mass over Eurasia appearing in the northern spring and summer climate. J Meteorol Soc Jpn 69(4):473–487

Zhang R, Wu B, Zhao P, Han J (2008) The decadal shift of the summer climate in the late 1980s over eastern China and its possible causes. Acta Meteorol Sin 22:435–445

Zhang R, Wu B, Han J, Zuo Z (2013) Effects on summer monsoon and rainfall change over China due to Eurasian snow cover and ocean thermal conditions. In: Singh BR (ed) Climate change – realities, impacts over ice cap, sea level and risks. InTech, Rijeka, 227–250

Zuo Z, Zhang R (2012) The anomalies of spring rainfall in China and its relation with tropical pacific SST and Eurasian snow. Chin J Atmos Sci 36(1):185–194

Zuo Z, Yang S, Wang W, Kumar A, Xue Y, Zhang R (2011) Relationship between anomalies of Eurasian snow and southern China rainfall in winter. Environ Res Lett 6:045402. doi:10.1088/1748-9326/6/4/045402

Zuo Z, Zhang R, Wu B et al (2012) Decadal variability in springtime snow over Eurasia: relation with circulation and possible influence on springtime rainfall over China. Int J Climatol 32(9):1336–1345

Zuo Z, Yang S, Hu ZZ, Zhang R, Wang W, Huang B, Wang F (2013) Predictable patterns and predictive skills of monsoon precipitation in northern hemisphere summer in NCEP CFSv2 reforecasts. Clim Dyn 40:3071–3088. doi:10.1007/s00382-013-1772-2

Zuo Z, Yang S, Zhang R et al (2014) Response of summer rainfall over China to spring snow anomalies over Siberia in the NCEP CFSv2 reforecast. Q J R Meteorol Soc 141:939–944. doi:10.1002/qj.2413